

Models of integrated magnetic components for simulation based design of SMPS with SIMPLORER

H. Njiende, H. Wetzel, N. Froehleke

Institute for Power Electronics and Electrical Drives
University of Paderborn, EIM -LEA
Pohlweg 47-49, 33098 Paderborn, Germany
e-mail: njiende@lea.upb.de

W. A. Cronje

Rand Afrikaans University
P.O. Box 524, Aucklandpark 2006,
South Africa
e-mail: wacronje@ieee.org

Acknowledgment

Thanks belong to ASCOM Energy Systems for partly funding this investigation within project "Low Voltage Power Supplies".

Keywords

<<Modeling, simulation, integrated magnetics, leakage inductances.>>

Abstract

A modeling approach of integrated magnetic components is presented. Analytical and FEM modeling results are compared to experimental results. The model of the integrated magnetic component allows a simplified integration into simulation tools enabling pre-optimization before breadboarding. This is shown by simulation and measured results for a push pull converter with current doubler rectifier.

1. Introduction

Voltage regulator modules (VRMs) are the prerequisite for proper operation of today's micro-electronics located in the proximity of microprocessors due to the challenging high power quality demands at high power density ratings. Lately introduced integrated magnetic components for VRMs as proposed in [3], [4] and [5] seems to be one key to fulfill latter requirements. Used in push pull forward converters with current-doubler rectifier, it showed to be an optimal solution for improving the topology efficiency and at the same time reducing volume and costs. Fig. 1 shows latter converter topology (see [1][2]). Three magnetic components are used in this topology variant: A 3-winding transformer and two filter inductors. Size and costs of these discrete components (as given in Fig. 2) and high voltage stress on power semiconductor components yield a negative impact, when compared to other double ended topologies. Additionally, the interconnections between transformer secondary

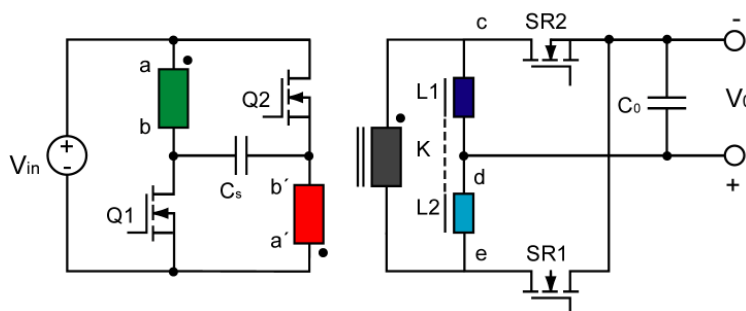


Fig. 1: Push Pull forward converter with built-in input filter and coupled inductor current doubler rectifier

and inductors, particularly at low voltage high current representing one target application for latter circuits cause extra losses.

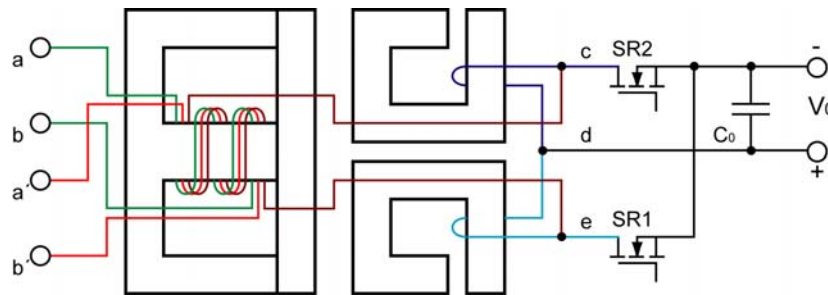


Fig. 2: Discrete magnetic components

Unluckily the above mentioned publications have the following shortcomings: The complete inductance or coupling coefficient matrix of the integrated magnetics is not outlined and discussed; the center air gap dependence of secondary windings coupling coefficient and output current ripple is misinterpreted and the effect of microscopic inherent outer air gaps is not considered at all. A modeling approach of integrated magnetic components is presented here, which is verified on a four winding component. Impacts of the center leg and outer leg air gaps on inductances, coupling factor and output current ripple are discussed. Analytical and FEM modeling results based on geometrical, material and winding data are compared to experimental results.

The complete modeling of the integrated magnetic component, also required for input and output filter design, leads to a simplified integration into simulation tools (here SIMPLORER¹ was used) enabling pre-optimization before breadboarding. This is viewed as one obstacle for the acceptance of the magnetic integration together with proposals based on exotic core manipulation in previous publications. A simulation approach, exemplary verified on a push pull converter with a built in input filter and coupled inductor, is presented here. A reluctance and electromagnetic model is derived for the transformer-inductor integrated component taking care of main and leakage fluxes. This in conjunction with simplified MOSFET models, which are easily up-dated by datasheets, ensures fast generation of simulation results. These are compared to measurements conducted on prototypes yielding satisfactory congruency.

2. Modeling of integrated magnetics

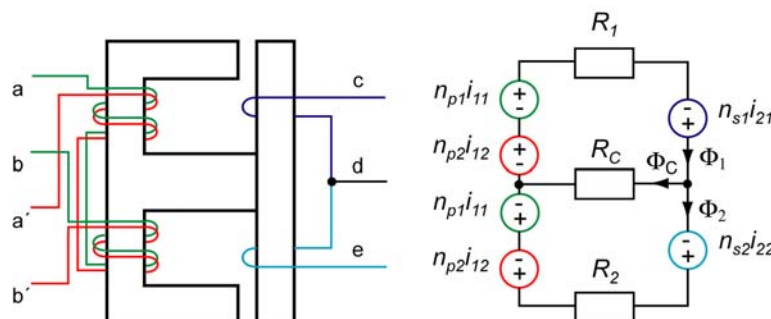


Fig. 3: Integrated magnetic component (air gaps in outer legs) and its corresponding reluctance model

¹ Product of Ansoft Corp.

In recent years several contributions were published on integrated magnetic components derivation from discrete components (Transformer and inductors) in order to lower volume and improve efficiency, [3][4][5]. Two different integrated magnetic components are addressed in this contribution.

- **Integrated component with air gaps in outer legs**

The magnetic reluctance model of the integrated component can be deduced from electric circuit model using the principle of duality. Applying Ampere's and Faraday's law and considering the flux continuity boundary condition to the magnetic circuit as depicted in Fig. 3 (where air gaps are located in the outer leg) yield the following matrix, which entirely describes the integrated component.

R_1 , R_2 and R_c are reluctances of outer legs and of center leg respectively. n_{p1} , n_{p2} , n_{s1} and n_{s2} are primary and secondary winding turns. Rows and columns of the matrix are of the order (p_1, p_2, s_1, s_2) .

For a symmetric structure (symmetric core: $R_1 = R_2 = R_0$ and symmetric primary and secondary windings: $n_{p1} = n_{p2} = \frac{n_p}{2}$ and $n_{s1} = n_{s2} = n_s$) the inductance matrix is simplified as shown above.

$$L = \begin{bmatrix} \frac{n_p^2}{2 \cdot R_{0c}} & \frac{n_p^2}{2 \cdot R_{0c}} & \frac{n_p \cdot n_s}{2 \cdot R_{0c}} & \frac{n_p \cdot n_s}{2 \cdot R_{0c}} \\ \frac{n_p^2}{2 \cdot R_{0c}} & \frac{n_p^2}{2 \cdot R_{0c}} & \frac{n_p \cdot n_s}{2 \cdot R_{0c}} & \frac{n_p \cdot n_s}{2 \cdot R_{0c}} \\ \frac{n_p \cdot n_s}{2 \cdot R_{0c}} & \frac{n_p \cdot n_s}{2 \cdot R_{0c}} & \frac{n_s^2 \cdot (R_0 + R_c)}{R_0(R_0 + 2 \cdot R_c)} & -\frac{n_s^2 \cdot R_c}{R_0(R_0 + 2 \cdot R_c)} \\ \frac{n_p \cdot n_s}{2 \cdot R_{0c}} & \frac{n_p \cdot n_s}{2 \cdot R_{0c}} & -\frac{n_s^2 \cdot R_c}{R_0(R_0 + 2 \cdot R_c)} & \frac{n_s^2 \cdot (R_0 + R_c)}{R_0(R_0 + 2 \cdot R_c)} \end{bmatrix} \quad (1)$$

where $R_{0c} = R_0 + 2 \cdot R_c$.

The coupling coefficient of both primary windings is one expressing the required essential tight coupling between these windings. A negative secondary mutual inductance gives evidence of inversely coupled secondary windings. Leakage inductance between both secondary windings calculated from Eq. 1 is given as follows:

$$Ll_{s1s2} = L_{s2s2} - L_{s1s2} = \frac{n_s^2}{R_0}. \quad (2)$$

- **Integrated component with air gap in center leg**

In order to reduce or even cancel flux ripple in the center leg and consequently reduce the core losses the polarity of one set of primary and secondary windings is changed.

Shifting the air gap into the center leg as depicted in Fig. 4 not only reduces the core losses, but enhances the mechanical stability of the structure and reduces EMI effects on adjacent components.

The repeated application of Ampere's and Faraday's law and consideration of the flux continuity boundary condition to the magnetic circuit in Fig. 4 yields

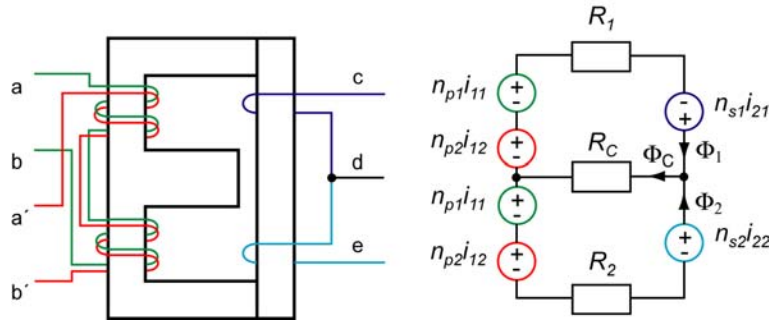


Fig. 4: Integrated magnetic component (air gap in center leg) and its corresponding reluctance model

$$L = \begin{bmatrix} \frac{n_p^2}{2 \cdot R_0} & \frac{n_p^2}{2 \cdot R_0} & \frac{n_p \cdot n_s}{2 \cdot R_0} & \frac{n_p \cdot n_s}{2 \cdot R_0} \\ \frac{n_p^2}{2 \cdot R_0} & \frac{n_p^2}{2 \cdot R_0} & \frac{n_p \cdot n_s}{2 \cdot R_0} & \frac{n_p \cdot n_s}{2 \cdot R_0} \\ \frac{n_p \cdot n_s}{2 \cdot R_0} & \frac{n_p \cdot n_s}{2 \cdot R_0} & \frac{n_s^2 \cdot (R_0 + R_c)}{R_0(R_0 + 2 \cdot R_c)} & \frac{n_s^2 \cdot R_c}{R_0(R_0 + 2 \cdot R_c)} \\ \frac{n_p \cdot n_s}{2 \cdot R_0} & \frac{n_p \cdot n_s}{2 \cdot R_0} & \frac{n_s^2 \cdot R_c}{R_0(R_0 + 2 \cdot R_c)} & \frac{n_s^2 \cdot (R_0 + R_c)}{R_0(R_0 + 2 \cdot R_c)} \end{bmatrix} \quad (3)$$

for a symmetric structure as depicted above.

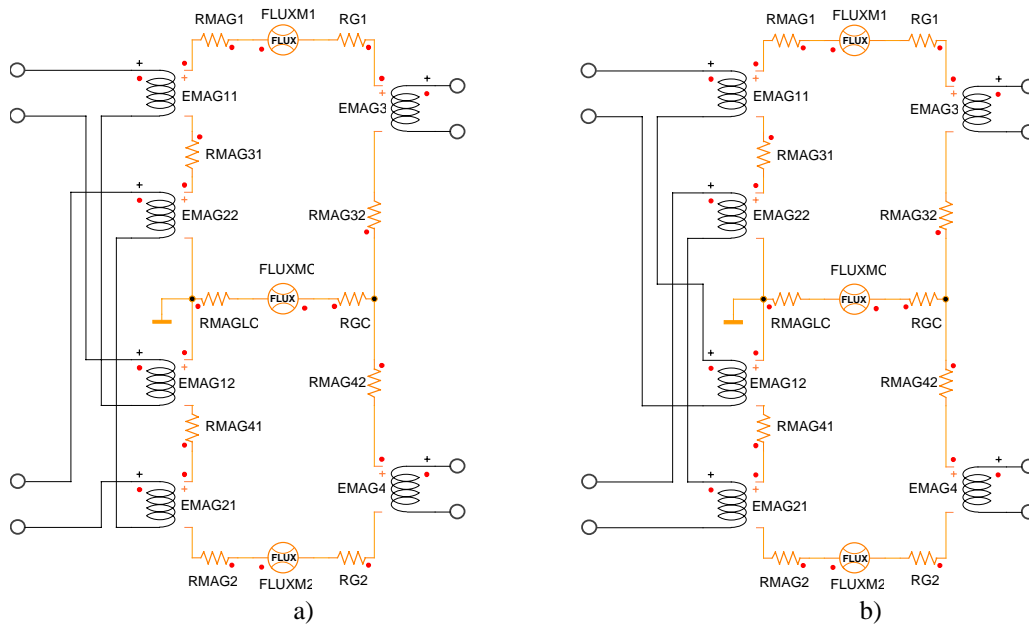


Fig. 5: Reluctance model in SIMPLORER for components of Fig. 3 and Fig. 4 without stray reluctances: a) with airgap in outer legs, b) with airgap in center leg

Leakage inductance between both secondary windings calculated from (3) are given as follows:

$$Ll_{s1s2} = L_{s2s2} - L_{s1s2} = \frac{n_s^2}{R_0 + 2 \cdot R_c} \cdot \quad (4)$$

An alternative is the modeling of integrated components using e.g. a SIMPLORER winding model, which represents (only) the coupled element between the electrical and magnetic equivalent circuit [6]. Hence the macro model includes two kinds of connections: Electrical and magnetic ones, see Fig. 5. It transfers electrical into magnetic energy and vice versa (bi-directional energy flow). The number of turns represents the coupling quantity between magnetic and electric domain.

- **Consideration of leakage inductances**

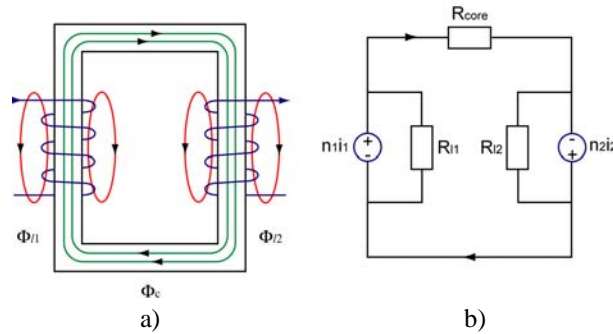


Fig. 6: a) Decomposition of magnetic fluxes into mutual and leakage fluxes and b) equivalent reluctance model

For a two winding transformer with current flowing in both windings, a typical flux distribution is shown in Fig. 2. The flux in each winding can be decomposed into two artificial parts: a mutual flux which links both windings and leakage fluxes which link only one winding respectively, see [7].

Considering this decomposition the total fluxes are as follows:

$$\phi_1(t) = \phi(t) + \phi_{11}(t) \quad (5)$$

$$\phi_2(t) = \phi(t) + \phi_{12}(t) \quad (6)$$

While the leakage fluxes considerably pass through air, the mutual inductance is mostly confined inside the core. Applying Faraday's Law yields the following equations:

$$\phi_{11} = \frac{n_1 i_1}{R_{11}} = P_{11} n_1 i_1, \quad (7)$$

$$\phi_{12} = \frac{n_2 i_2}{R_2} = P_2 n_2 i_2 \quad \text{and} \quad (8)$$

$$\phi = \frac{(n_1 i_1 + n_2 i_2)}{R_{core}} = P_{core} \cdot (n_1 i_1 + n_2 i_2) \quad (9)$$

where P_{11} , P_{12} , and P_{core} are primary side, secondary side stray and core (or mutual) permeances respectively. R_{11} , R_{12} , and R_{core} are the respective reluctances.

Substituting the last three equations in Faraday's Law yields the following

$$v_1 = L_{11} \cdot \dot{i}_1 + M_{12} \cdot \dot{i}_2 \quad (10)$$

$$v_2 = M_{12} \cdot \dot{i}_1 + L_{22} \cdot \dot{i}_2, \quad (11)$$

where

$$L_{11} = n_1^2 \cdot (p_{l1} + p_{core}), \quad (12)$$

$$L_{22} = n_2^2 \cdot (p_{l2} + p_{core}) \text{ and} \quad (13)$$

$$M_{12} = n_1 n_2 \cdot p_{core}. \quad (14)$$

Subsequently it can be followed for a transformer with several windings, that the self inductance of a given winding is the sum of the principal (in core) inductance and all stray inductances linking all other winding combinations to this winding. In case of a four winding transformer the self and mutual inductances are given as follows:

$$L_{p_1 p_1} = n_{p_1}^2 \cdot (p_{l p_1} + p_{l p_1 p_2} + p_{l p_1 s_1} + p_{l p_1 s_2} + p_{l p_1 p_2 s_1} + p_{l p_1 p_2 s_2} + p_{l p_1 s_1 s_2} + p_{core}) \quad (15)$$

$$M_{p_1 p_2} = n_{p_1} \cdot n_{p_2} \cdot (p_{l p_1 p_2} + p_{l p_1 p_2 s_1} + p_{l p_1 p_2 s_2} + p_{core}) \quad (16)$$

The remaining elements of the inductance matrix can be calculated accordingly.

For push pull forward converters; both primary windings are tightly coupled, primary windings are split in two, every side of split primary winding is strongly coupled with a secondary winding and they are interleaved to reduce leakages. Considering these facts the inductances can be simplified to:

$$L_{pp} \approx n_p^2 \cdot (p_{l p_1 p_2 s_1} + p_{l p_1 p_2 s_2} + p_{core}) \quad (17)$$

$$M_{pp} \approx n_p^2 \cdot (p_{l p_1 p_2 s_1} + p_{l p_1 p_2 s_2} + p_{core}) \quad (18)$$

$$L_{ss} \approx n_s^2 \cdot (p_{l p_1 p_2 s_1} + p_{core}) \approx n_s^2 \cdot (p_{l p_1 p_2 s_2} + p_{core}) \quad (19)$$

$$M_{ps} \approx n_p \cdot n_s \cdot (p_{l p_1 p_2 s_1} + p_{core}) \approx n_p \cdot n_s \cdot (p_{l p_1 p_2 s_2} + p_{core}) \quad (20)$$

$$M_{ss} \approx n_s^2 \cdot p_{core} \quad (21)$$

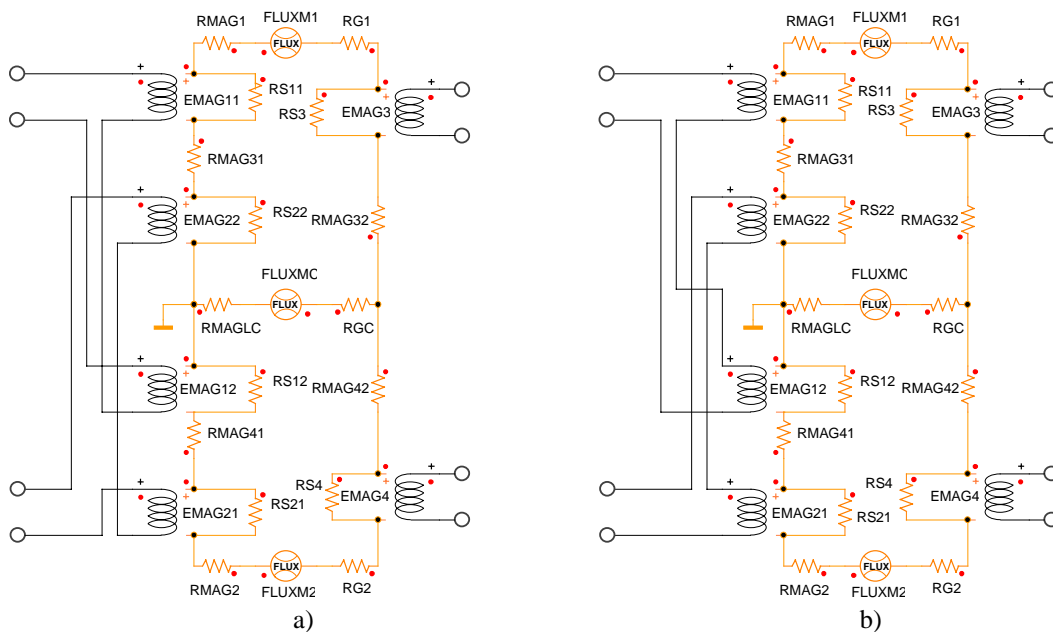


Fig. 7: Reluctance model in SIMPLORER with stray reluctances
a) with air gaps in outer legs and b) with air gap in center leg

The leakage inductances are calculated under following assumptions: there is no skin effect in windings, the excitation magnitude H is zero in the core and the field lines in the window are rectilinear. The leakage permeance (inverse value of reluctance) between two windings is calculated as follows:

$$P_{leak} \approx \frac{\mu_0 \cdot \lambda \cdot \left(\frac{d_{cu}}{3} + d \right)}{W} \cdot \frac{1}{N_w^2} \quad (22)$$

where W represents the width of the planar winding, λ the mean-length of the winding, d the total interwinding spacing and d_{cu} the total copper thickness. The interleaving of split windings is accounted for by N_w , which is the number of interfaces (equals number of packed windings minus one).

For a more detailed model of the integrated magnetic component by adding stray reluctances are considered, which according to Fig. 6 are set in parallel to magnetomotive forces (mmf). The models for the components are given in Fig. 7.

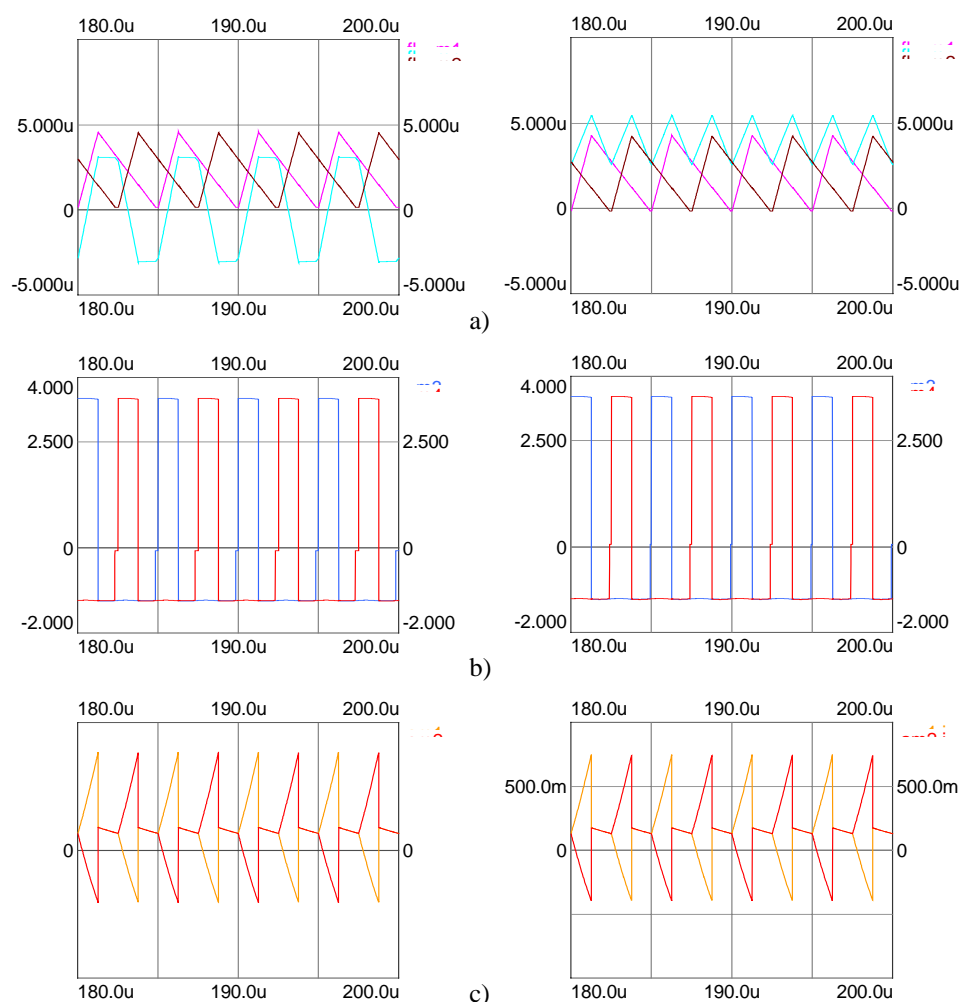


Fig. 8: Simulation results: a) Magnetic fluxes in all core legs, b) secondary winding voltages and c) primary winding currents respectively for configurations in Fig. 3 (left) and Fig. 4 (right)

A simulation of a push pull forward converter with current doubler rectifier is carried out with the models shown in Fig. 7. While primary winding currents and secondary winding voltage for both configurations of magnetic component are practically unchanged there a drastic flux ripple reduction using the structure in Fig. 4, which is one of most important benefits.

Semiconductors (Diodes and MOSFET) are considered ideal for generation of the above simulation results. The leakage capacitances are not considered.

3. Analysis of the integrated component

The structure of the matrix L exhibits that all but the secondary inductances (self and mutual of both) are independent of the center leg and of the air gap of the center leg. The coupling factor of both primary windings is one, since they are tightly wound (bifilar for solenoidal component). In the underlying integrated component the main gap is allocated to the center leg, Fig.4. This leads to a much larger reluctance in the center leg than those in the outer legs, resulting only from the polishing process of the surface of the core halves. Note, the self inductances of these windings are utilized as filter inductance.

Using the geometry of the core, reluctances can be computed and moreover inductance and coupling coefficient matrices. The dependence of inductances on the air gaps in outer and center gap is illustrated in Fig. 9 a) and b). Note that the secondary inductors coupling coefficient rise with the center leg air gap. The output current ripple is only related to the leakage inductance of two coupled secondary inductors (as stated in [4]):

$$Ll_{s1s2} = \frac{n_s^2}{R_0} \cdot \frac{1 - K_{ss}}{1 + K_{ss}}, \quad (23)$$

$$\Delta i_o = \frac{2 \cdot V_o}{Ll_{s1s2} \cdot f_s} \cdot (1 - D) \quad (24)$$

where K_{ss} is the secondary coupling factor, V_o the output voltage, f_s the switching frequency and D the duty cycle.

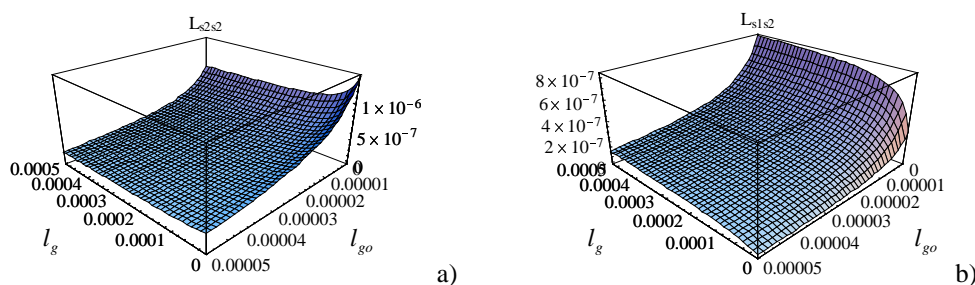


Fig. 9: Self L_{s2s2} a) and mutual inductances L_{s1s2} b) versus center- (l_g) and outer leg air gaps (l_{go})

4. Design Considerations and Experimental Results

The integrated magnetic components of approx. 300 nH output inductance were built for a 48V- input, 1.6V/15A output push pull forward converter with current doubler rectifier operated at a switching frequency of 200 kHz.

An optimization according to [8] yields a planar device using ELP22/ELP22 cores of EPCOS with a

configuration of single turn secondary windings and twenty turn primary windings. Depicted analytical results match quite well the FEM results as well as the measurement results of built prototype.

$$L_{analyt} = \begin{bmatrix} 435 & 435 & 21.75 & 21.75 \\ 435 & 435 & 21.75 & 21.75 \\ 21.75 & 21.75 & 1.28 & 0.89 \\ 21.75 & 21.75 & 0.89 & 1.28 \end{bmatrix} \mu H$$

$$L_{FEM} = \begin{bmatrix} 402 & 402.5 & 20.25 & 20.25 \\ 402.5 & 402 & 20.25 & 20.25 \\ 20.25 & 20.25 & 1.12 & 0.887 \\ 20.25 & 20.25 & 0.887 & 1.12 \end{bmatrix} \mu H$$

$$L_{meas} = \begin{bmatrix} 431 & 533 & 24.82 & 24.22 \\ 533 & 433 & 25.15 & 21.82 \\ 24.82 & 25.15 & 1.3 & 0.98 \\ 24.22 & 21.82 & 0.98 & 1.28 \end{bmatrix} \mu H$$



Fig. 10: Analytical, FEM and measurement results of built planar component

The whole circuit including above mentioned integrated magnetic component and MOSFET model including dominant parasitic capacitances is inserted in a SIMPLORER sheet. Simulated and measured gate, drain-source voltage of a primary sided MOSFET, input current and output current are illustrated in Fig. 11. Simulation and measurement results match reasonably. The different oscillations appearing in measured and simulated drain source voltage are due to not sufficiently accurate modeling of leakage inductances of the integrated magnetics and especially neglect of damping via skin effect. Oscillations in the measured input current are caused by parasitic resonance (capacitances and leakage inductances of PCB and magnetic component).

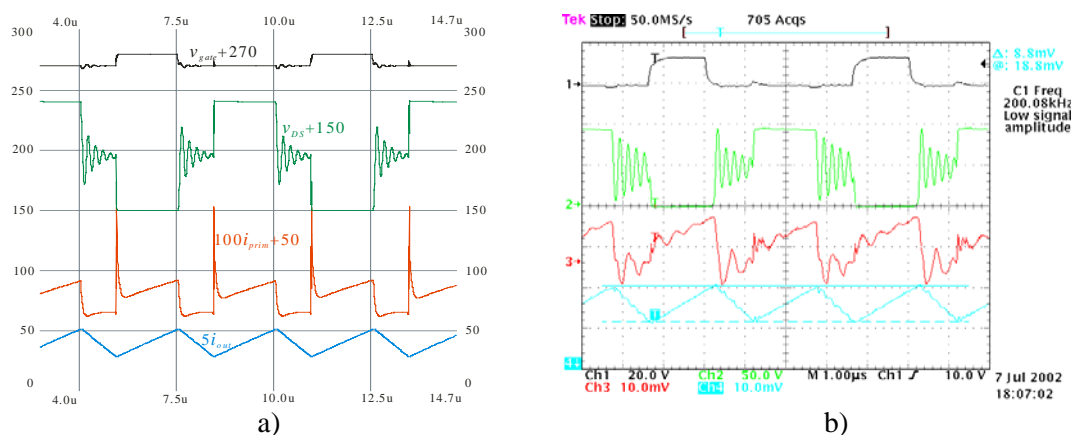


Fig. 11: Gate (v_{gate} , Ch1) and drain source voltage (v_{DS} , Ch2), input (i_{prim} , Ch3, 0.5A/div) and output current (i_{out} , Ch4, 5A/div)

5. Conclusion and outlook

Modeling approaches of integrated magnetic components based on reluctances and electromagnetic coupled elements are presented. Leakage inductances are accounted for by inserting equivalent reluctances parallel to the mmf's. Analytical and FEM modeling results are compared to experimental results. The model of the integrated magnetic component allows a simplified integration into

simulation tools enabling pre-optimization before breadboarding. This is shown by simulation and measured results for a push pull converter with current doubler rectifier.

Inclusion of structural capacitances will allow forecasting of voltage stresses resulting from ringing phenomena more precisely and utilize them in integrated power electronic modules. By consideration of skin and proximity effects the damping deviations could be reduced.

6. References

- [1] W. Chen, G. Hua, D. Sable, F. C. Lee, "Design of High efficiency, low profile, low voltage converter with integrated Magnetics," IEEE APEC, 1997, pp. 911-917.
- [2] P. Wong, Q. Wu, P. Xu, B. Yang and F.C. Lee, "Investigating Coupling Inductor in Interleaving QSW VRM," IEEE APEC, 2000, pp. 973-978.
- [3] P. Xu, Q. Wu, P. Wong, and F. C. Lee, "A Novel Integrated Current- Doubler Rectifier," IEEE APEC, 2000.
- [4] P. Xu and F.C. Lee, "Design of High-Input Voltage Regulator Modules With A Novel Integrated Magnetics," IEEE APEC, 2001.
- [5] P. Xu, M. Ye and F. C. Lee, "Single Magnetic Push-Pull Forward Converter Featuring Built-in Input Filter and Coupled-Inductor Current Doubler for 48V VRM," IEEE APEC, 2002.
- [6] Ansoft, "SIMPLORER v 6.0 User Manual", 2002.
- [7] S.-P. Hsi, R. D. Middlebrook and S. Cuk, "Transformer Modelling and Design for Leakage Control," Advances in switched Mode Power Conversion, Volume II, Pasadena, USA, 1981.
- [8] N. Froehleke, H. Munding, H. Njiende, P. Wallmeier, H. Puder, "CAE-Tool for Optimizing Development of Switched Mode Power Supplies," IEEE APEC, 2001.